

20. Techniques for Ultrafast Spectroscopy

John T. Fourkas

Ultrafast Spectroscopy

In this chapter we discuss commonly used ultrafast spectroscopic techniques, how they are implemented, and what they can be used to measure. The list of techniques in this chapter is not intended to be exhaustive, but rather to give the reader a feel for the methods that are used most frequently. Specific applications of these techniques and discussions of more advanced techniques can be found in subsequent chapters.

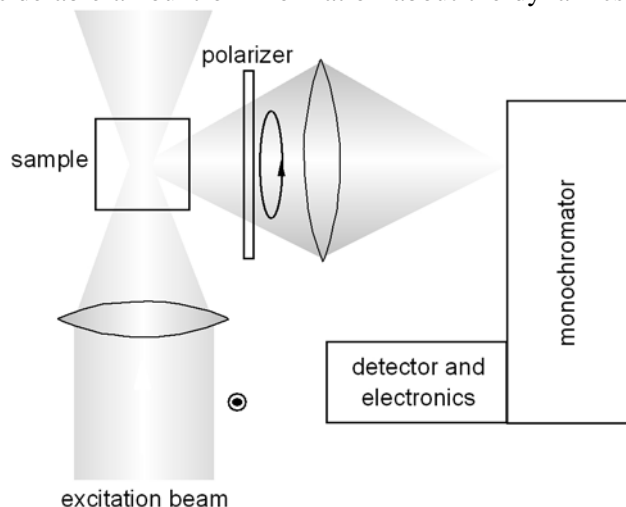
Time-Resolved Fluorescence Spectroscopy

Probably the simplest ultrafast experiment involves exciting a sample with a pulse of light and monitoring its incoherent emission of light as a function of time. Ultrafast pulses are most useful for such an experiment when the emission time scale is longer than the pulse duration by anywhere from one to several orders of magnitude. Based on this criterion, ultrafast pulses are useful for monitoring fluorescence from atoms or molecules, which generally has a lifetime in the range of a few picoseconds to a few nanoseconds. Luminescence from semiconductors, metals, and other solid-state materials also can occur on time scales that are appropriate for this technique.

In a typical time-resolved fluorescence experiment (Fig. 20.1), [1, 2] a solution of a molecule of interest is held in a square cuvette. A low concentration is employed to prevent reabsorption of the fluorescence by unexcited molecules. A train of excitation pulses enters the cuvette normal to one of its faces. The polarization of the excitation pulses is usually vertical. The spacing between the pulses must be at least several times the fluorescence lifetime so that virtually no molecules are in the excited state when any pulse arrives. A typical Ti:sapphire laser has a repetition rate on the order of 80 MHz, corresponding to an interpulse delay time of 12.5 ns. Thus, for molecules with fluorescence lifetimes that are greater than approximately 4 ns, it is necessary to use a pulse picker to lower the effective repetition rate of excitation. It may also be necessary to flow the sample if, for instance, the molecules have a long-lived triplet state or can undergo an irreversible reaction from the excited state.

20. Techniques for Ultrafast Spectroscopy

Fluorescence is collected from another face of the cuvette that is perpendicular to the input face. The collected light often passes through a polarizer, and may also pass through a monochromator before being collected by a high-efficiency detector. In the most complete experiment it is therefore possible to determine the fluorescence intensity as a function of wavelength, polarization, and time following excitation. As we will see, such data can provide a considerable amount of information about the dynamics of the mole-



cules of interest.

Fig. 20.1. Schematic of a typical time-resolved fluorescence setup. The excitation light is polarized vertically, and the detection polarization is controlled with an adjustable polarizer in the collection path. The monochromator is used to determine the range of wavelengths over which fluorescence is collected.

The most commonly used method for time-resolving fluorescence decays is time-correlated single-photon counting.[3, 4] In this technique a highly sensitive, fast detector called a microchannel plate photomultiplier is used to detect single fluorescence photons. A small portion of each excitation pulse is picked off and sent to a photodiode to create an electronic signal that represents zero delay time. The arrival times of photons are measured electronically relative to this “start” pulse. For this technique to work well, it is crucial that at most one fluorescence photon be collected per excitation pulse. To ensure that this criterion is met, low enough excitation powers are employed that one photon is collected for every hundred or even every thousand laser pulses.

One of the advantages of time-correlated single-photon counting is that it is a completely electronic technique, and so it is relatively straightforward to implement. However, by the same token, as an electronic technique it offers only limited time resolution, typically on the order of tens to hun-

dreds of picoseconds. In addition, the low intensities required to ensure that at most one photon is detected per excitation pulse limit the rate of data acquisition.

An alternative detection technique is fluorescence upconversion.[5, 6] In this technique the timing of fluorescence is measured optically. The fluorescence is directed to a nonlinear crystal where it is mixed with a portion of the output of the excitation laser, which is known as the “gate” pulse. Light is then detected at the sum of the excitation and fluorescence frequencies. The decay of the fluorescence is determined by scanning the gate pulse relative to the excitation pulse. Because the gate pulse has the same duration as the excitation pulse, superb time resolution can be achieved. So long as the laser pulses are short enough and the nonlinear crystal is thin enough, it is possible to attain time resolutions on the order of 100 fs.

The sum-frequency generation process works best when there are many fluorescence photons. This means that in highly fluorescent samples the data acquisition rate can be fast, but conversely in weakly fluorescent samples data collection is slow. To achieve the best possible time and frequency resolution, thin nonlinear crystals must be employed. However, such crystals decrease the magnitude of the upconversion signal. The alignment of the optics for fluorescence upconversion can also be considerably trickier than for time-correlated single-photon counting.

The intrinsic radiative lifetime of molecules, τ_r , is generally on the order of nanoseconds to tens of nanoseconds. The radiative rate constant, k_r , is the inverse of τ_r . In most molecules there are competing, non-radiative processes that remove population from the excited state. Such non-radiative processes can include, but are not limited to, intersystem crossing to a triplet state, internal conversion to a different singlet state, electron transfer, and other photochemical reactions. If all of these processes are unimolecular (such their rates depend only upon the excited-state population), then the fluorescence intensity as a function of time after excitation is given by:

$$I_r(t) \propto \frac{k_r}{k_r + \sum_i k_{nr,i}} [E]_0 \exp\left[-\left(k_r + \sum_i k_{nr,i}\right)t\right], \quad (20.1)$$

where the $k_{nr,i}$ are the rate constants for all of the competing non-radiative processes and $[E]_0$ is the initial concentration of excited-state molecules. Note that the observed radiative lifetime is given by:

$$\tau_{r,obs} = \left(k_r + \sum_i k_{nr,i}\right)^{-1}. \quad (20.2)$$

Thus, while the fluorescence emission often decays exponentially in time, the observed radiative decay time may vary considerably from the intrinsic value of τ_r .

The leading term on the right side of Eq. (20.1) is the ratio of the radiative decay rate to the total decay rate of the excited state, which is also

equivalent to the fraction of molecules that fluoresce after being excited. As a result, this fraction is known as the fluorescence quantum yield, which is often denoted Φ_f . Note that the denominator in Φ_f is equal to the observed radiative rate constant. This means that if the total emitted fluorescence intensity and $[E]_0$ can be determined, it is possible to back out the intrinsic radiative rate constant from the time-resolved fluorescence decay. Determining $I_r(t)$ requires knowing parameters such as the total solid angle over which fluorescence is collected and the efficiency of the detection system. $[E]_0$ can be determined from knowledge of the absorption cross section of the molecules at the excitation wavelength, the intensity of the excitation, and the volume of the sample from which fluorescence is collected. Due to the inherent uncertainty in determining Φ_f , it is challenging (but not impossible) to determine τ_r with high accuracy from time-resolved fluorescence decays. Once τ_r is known it is possible to glean information about the rates of non-radiative decay processes in the system as well.

The time dependence of the detected fluorescence can also be affected by the reorientation of molecules. Recall that the excitation light is generally vertically polarized. The normalized probability distribution of excited molecules is then $P(\theta, \varphi) \sin\theta d\theta d\varphi = (3/4\pi)\cos^2\theta \sin\theta d\theta d\varphi$, where θ is the angle that the excitation transition dipole of the molecule makes with the vertical axis. The polarization of the detected light is in the y - z plane. It can then be shown that for our initial distribution of excited molecules, the relative intensity detected at zero delay time with the polarizer set at a particular angle χ to the z axis is given by:[7]

$$I(0, \chi) = \frac{1}{5}(1 + 2\cos^2 \chi). \quad (20.3)$$

At long enough delay times the orientational distribution of excited molecules becomes isotropic, i.e. $P(\theta, \varphi) \sin\theta d\theta d\varphi = (1/4\pi) \sin\theta d\theta d\varphi$. We find in this limit that

$$I(t \gg \tau_{or}, \chi) = \frac{1}{3} \exp(-t/\tau_{r,obs}), \quad (20.4)$$

where τ_{or} is the orientational correlation time of the molecules. Note that, as should be expected, this result does not depend on χ .

Two important special cases of detection polarization are vertical (which, since the excitation polarization is vertical, is denoted as \parallel or VV) and horizontal (which is denoted \perp or VH). In the former case, according to Eq. (20.3) the relative intensity at zero time is given by $I_{\parallel}(0) = 3/5$. In the latter case, the relative intensity at zero time is given by $I_{\perp}(0) = 1/5$. Thus, orientational diffusion will cause $I_{\parallel}(t)/\exp(-t/\tau_{r,obs})$ to decay from an initial relative value of 3/5 to one of 1/3 at long time and similarly will cause $I_{\perp}(t)/\exp(-t/\tau_{r,obs})$ to increase from an initial relative value of 1/5 to one of 1/3 at long times. Under most circumstances, including that of isotropic orientational

20. Techniques for Ultrafast Spectroscopy

diffusion, the changes in $I_{\parallel}(t)/\exp(-t/\tau_{r,obs})$ and $I_{\perp}(t)/\exp(-t/\tau_{r,obs})$ are monotonic.

It is convenient to define a time-dependent quantity $r(t)$ that is known as the fluorescence anisotropy:

$$r(t) = \frac{I_{\parallel}(t) - I_{\perp}(t)}{I_{\parallel}(t) + 2I_{\perp}(t)}. \quad (20.5)$$

Note that because $r(t)$ is a ratio of intensities, the $\exp(-t/\tau_{r,obs})$ term is divided out. The decay of the fluorescence anisotropy is a direct measure of the orientational correlation time(s) of the molecules. In the simplest case, in which molecules reorient isotropically with a single orientational diffusion constant, $r(t)$ will decay exponentially with time constant τ_{or} . Molecules that have anisotropic diffusion tensors can exhibit multi-exponential decays, and even greater complexity is added when the transition dipole moment is not parallel to one of the principal axes of the diffusion tensor.

Note that Eq. (20.5) predicts that $r(0)$ should take on a value of 0.4. However, the initial anisotropy is often observed to take on values smaller than 0.4. There are many possible sources for this reduction in $r(0)$. For instance, depending on how the fluorescence decay is time resolved, the time resolution can be as short as the length of the pulses employed or as long as tens to hundreds of picoseconds. Any dynamic processes that occur on a time scale that is faster than the resolution of the apparatus will lower the apparent initial value of $r(t)$. As another example, in the above derivation we assumed that the excitation and emission transition dipoles are identical. However, they need not be, and if they are not at least parallel to one another then $r(0)$ will take on a value less than 0.4.[7]

Whereas $r(t)$ makes it possible to study reorientation while removing the effects of lifetime decay, it is also desirable to be able to do the converse, i.e. to measure the lifetime decay without any influence from the reorientation of molecules. This goal can be accomplished by choosing a polarization angle χ such that $I(0,\chi) = I(t \gg \tau_{or})/\exp(-t/\tau_{r,obs})$. Inspection of Eqs. (20.3) and (20.4) shows that this condition is met when $\cos^2\chi = 1/3$, in which case $\chi = 54.7^\circ$. By setting the detection polarizer to this “magic angle” it is possible to isolate the lifetime contribution of the fluorescence decay.

In the above discussion of the decay of the time-resolved fluorescence signal, we have assumed that the light was collected across the entire fluorescence spectrum. If the fluorescence is instead collected over a small range of wavelengths, the observed decay may not be exponential or even monotonic. Furthermore, the shape of the decay depends on the set of wavelengths being monitored. In other words, the fluorescence spectrum can change both shape and position as a function of time after excitation.

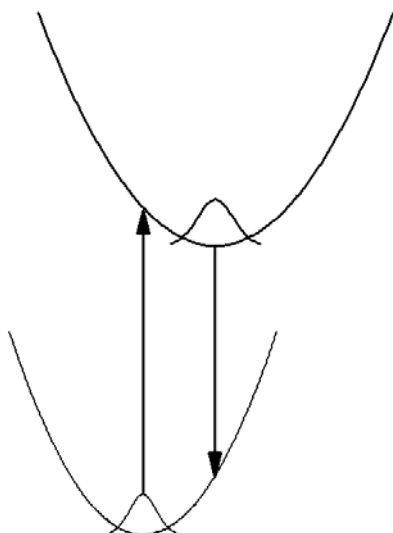


Fig. 20.2. The source of time-dependent fluorescence spectra in solution. The solvent is initially in equilibrium with the ground-state fluorophores. The excitation process (upward arrow) is essentially instantaneous, after which the solvent readjusts to the excited-state species, simultaneously stabilizing the excited state and destabilizing the ground state. As a result, fluorescence (down arrow) red shifts as a function of time after excitation until the solvent has equilibrated about the excited state.

One potential cause for the time-dependence of the fluorescence spectrum is the existence of more than one fluorescent state of a molecule, which can arise, for instance, from multiple excited-state structures. However, this phenomenon is generally observed even in molecules with a single fluorescent state due to the dynamics of the surrounding solvent (Fig. 20.2). When the fluorophores are initially in the ground state, the solvent has equilibrated itself around them. Electronic excitation changes properties of the fluorophores such as the dipole moment, the polarizability, and even the shape and size. As a result, immediately following excitation the solvent structure is not equilibrated to the new properties of the solute. As the solvent adjusts itself to accommodate the excited-state solute, the energy of the solute is lowered. The more the solvent structure adjusts itself to accommodate the excited solute, the farther it is from a structure that stabilizes a ground-state solute. Thus, while the excited state is being stabilized the ground state is being destabilized, and as a result the fluorescence spectrum shifts to the red as a function of time after excitation until such time as the excited state has been fully stabilized. If the “solvation potentials” in the ground and excited states differ in their curvature, then the width of the fluo-

rescence spectrum may change as a function of time after excitation as well. Probing such solvation dynamics is a common application of time-resolved fluorescence spectroscopy.[8-11]

Pump/Probe Spectroscopy

We now turn to nonlinear ultrafast spectroscopies,[12] the simplest of which is pump/probe spectroscopy.[13, 14] The basic idea of this technique is that one ultrafast pulse (the pump) is used to affect a system of interest and a second pulse (the probe), which arrives at a variable delay time, is used to probe how the system has been altered by the pump pulse. The two pulses can come from the same laser from different lasers. In the latter case the pulses can be of different colors, providing added flexibility but increased experimental complexity. The probe pulse can interrogate the time dependence of a pump-induced change in the sample's absorption, stimulated emission, refractive index, reflectivity, or some combination of all of four.

A typical pump/probe experimental setup is shown in Fig. 20.3. The output of an ultrafast laser is divided into an intense pump beam and a weaker probe beam using a beam splitter. One of the beams traverses a computer-controlled delay line to control the timing between the pulses. The beams may also pass through additional optics to control intensity and/or polarization. The beams usually are made parallel and then pass through symmetrical positions on the opposite sides of the center of a single lens that focuses them into the sample. The probe beam may pass through one or more spatial filters and/or a monochromator following the sample, after which it is incident on a slow detector. Data collection involves monitoring the probe beam intensity as a function of the delay time between the pump and probe pulses. To improve the signal-to-noise ratio of the experiment, the pump beam can be chopped and the detector can be connected to a lock-in amplifier that is referenced to the chopping frequency. Alternatively, the pump and probe beams can both be chopped at different frequencies, and the lock-in can be referenced to the sum or the difference of the chopping frequencies.

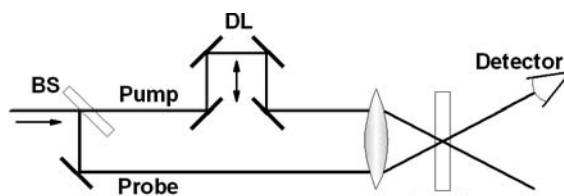


Fig. 20.3. Schematic of a typical experimental setup for pump/probe spectroscopy. BS = beam splitter, DL = delay line.

20. Techniques for Ultrafast Spectroscopy

We begin by considering changes in absorption and/or stimulated emission. In most cases, the atoms or molecules under study begin in their electronic ground states (Fig. 20.4). Absorption will be strong at wavelengths that correspond to allowed transitions between these ground states and excited states. After the pump pulse induces absorption, three effects influence the transmission of the probe beam. First, there is a depletion in the ground-state population, which decreases absorption. Second, there is now excited-state population that can be stimulated back down to the ground state, causing *gain* in the probe pulse if it is at the appropriate wavelength. Third, the excited-state population can also be driven to higher excited states if the probe pulse is in resonance with allowed excited-state/ground-state transitions. Which of these effects play an important role in pump/probe spectroscopy depend both on the dynamics of the molecule and on the excitation and probe wavelengths.

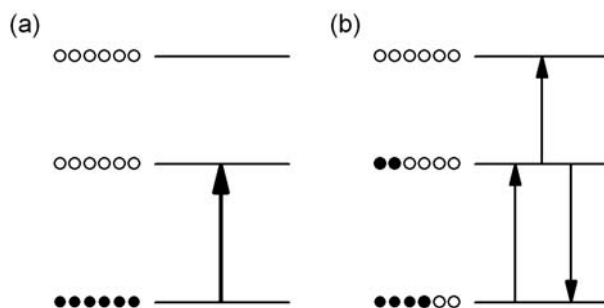


Fig. 20.4. Energy-level scheme for transient absorption spectroscopy. (a) All of the population begins in the ground electronic state. (b) The pump pulse transfers some population to an excited electronic state, leading to a bleach in the ground-state absorption, stimulated emission from the electronic excited state, and absorption from the electronic excited state to higher excited states.

Let's take a look at the effect of the reduction in the ground-state population on the transmission of the probe beam. The absorbance A of a sample is given by

$$A = \alpha(\lambda)c_{gs}\ell \quad , \quad (20.6)$$

where $\alpha(\lambda)$ is the absorption coefficient at the probe wavelength λ , c_{gs} is the concentration of ground-state species, and ℓ is the path length. The pump pulse decreases the initial concentration of ground-state species, c_{gs}^0 by $\Delta c_{gs}(\tau)$, where τ is the delay time; note that for low to moderate pump intensities, we expect that $\Delta c_{gs}(0) \propto I_{pump}$. We will assume that for positive delay times the concentration of ground-state molecules recovers exponentially with time constant τ_{gs} , so that

20. Techniques for Ultrafast Spectroscopy

$$c_{gs}(\tau \geq 0) = c_{gs}^0 - \Delta c_{gs} \exp(-\tau / \tau_{gs}) \quad . \quad (20.7)$$

The transmitted intensity is then given by

$$\begin{aligned} I_{tr}(\lambda, \tau \geq 0) &= I_0(\lambda) \exp\left\{-\alpha(\lambda) \ell \left[c_{gs}^0 - \Delta c_{gs} \exp(-\tau / \tau_{gs}) \right]\right\} \\ &= I_0(\lambda) \exp\left(\alpha(\lambda) c_{gs}^0 \ell\right) \\ &\quad \times \exp\left\{\alpha(\lambda) \Delta c_{gs} \ell \exp(-\tau / \tau_{gs})\right\} \quad . \quad (20.8) \end{aligned}$$

If we now assume that $\alpha(\lambda) \Delta c_{gs} \ell \ll 1$, we find

$$\frac{I_{tr}(\lambda, \tau \geq 0)}{I_{tr}(\lambda, \tau < 0)} \cong 1 + \alpha(\lambda) \Delta c_{gs} \ell \exp(-\tau / \tau_{gs}) \quad . \quad (20.9)$$

In other words, the fractional increase in probe transmission due to the ground-state bleach is given by

$$\frac{\Delta I_{gsb}(\lambda, \tau)}{I_0(\lambda)} = \alpha(\lambda) \Delta c_{gs} \ell \exp(-\tau / \tau_{gs}) \quad . \quad (20.10)$$

The ‘‘hole’’ in the ground state therefore results in an increase in transmission that decays exponentially with time constant τ_{gs} as population returns to the ground state.

Stimulated emission similarly depends upon the change in the excited-state population induced by the pump pulse, Δc_{es} . Note that in the simplest case $\Delta c_{gs} = \Delta c_{es}$, but if other states (such as triplets) are involved then these quantities will not be equal. By logic analogous to the above, the fractional increase in probe transmission due to stimulated emission is given by

$$\frac{\Delta I_{se}(\lambda, \tau)}{I_0(\lambda)} = \alpha_{se}(\lambda) \Delta c_{es} \ell \exp(-\tau / \tau_{es}) \quad , \quad (20.11)$$

where τ_{es} is the excited-state lifetime and α_{se} is analogous to the absorption coefficient.

While the ground-state bleach and stimulated emission serve to increase the probe transmission, absorption between excited states decreases the transmission. In this case we find that

$$\frac{\Delta I_{ea}(\lambda, \tau)}{I_0(\lambda)} = -\alpha_{ea}(\lambda) \Delta c_{es} \ell \exp(-\tau / \tau_{es}) \quad , \quad (20.12)$$

where α_{ea} is the absorption coefficient for excited-state absorption.

Putting all of these pieces together we find that the pump/probe signal is given by

$$\begin{aligned} S(\tau, \lambda) &\propto \ell \left\{ \alpha(\lambda) \Delta c_{gs} \exp(-\tau / \tau_{gs}) \right. \\ &\quad \left. + [\alpha_{se}(\lambda) - \alpha_{ea}(\lambda)] \Delta c_{es} \exp(-\tau / \tau_{es}) \right\} \quad (20.13) \end{aligned}$$

Of course, the decay dynamics can be considerably more complex than depicted here, due both to the involvement of other states and to effects such as the solvation dynamics discussed above. Shown in Fig. 20.5 is a schematic depiction of the appearance of a transient absorption spectrum from a pump-probe experiment in which all three of the above contributions are identified.

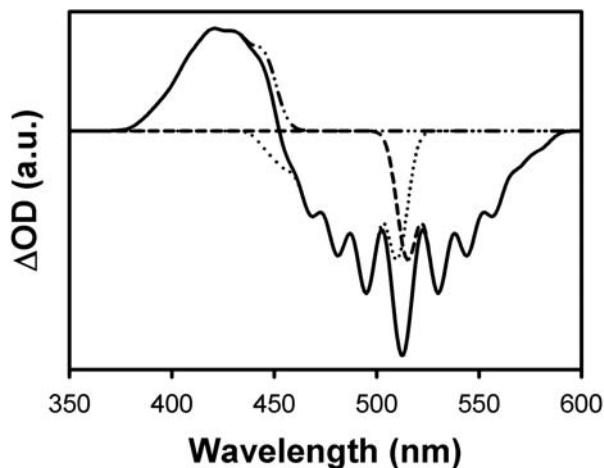


Fig. 20.5. Schematic depiction of a transient absorption spectrum. The solid line represents the total spectrum, the dotted line represents the absorption bleach component, the dashed line represents the stimulated emission component, and the dashed-and-dotted line represents excited-state absorption.

In addition to information concerning the dynamics of electronic states, pump/probe experiments can also be used to monitor vibrational dynamics. Consider a molecule for which there are two vibronic levels in the excited state, $|e_1\rangle$ and $|e_2\rangle$, that are within the bandwidth of the pump pulse (Fig. 20.6). The pump pulse can then create a coherence between these two states that evolves at frequency $\omega_{21} = [E(e_2) - E(e_1)]/\hbar$, imposing oscillations on the signal at this frequency. The decay rate of the oscillations can be related to the rate of vibrational dephasing.

Polarization can also play an important role in pump/probe spectroscopy. All of the polarization tricks discussed above for time-resolved fluorescence spectroscopy can also be used in pump/probe spectroscopy. For instance, decays in which the pump and probe beams have the same polarization can be combined with decays in which they have orthogonal polarizations to determine the time-dependent anisotropy and thereby gain information on orientational dynamics. In addition, probing at the magic angle relative to the pump polarization allows the effects of reorientation to be removed from the decay entirely.

20. Techniques for Ultrafast Spectroscopy

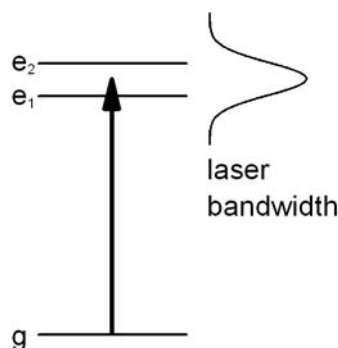


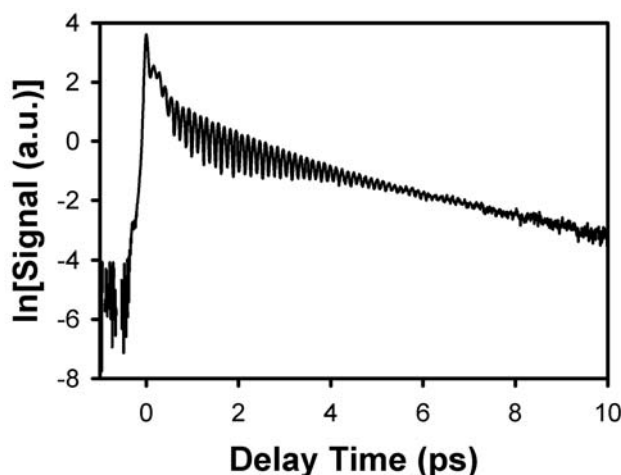
Fig. 20.6. Energy-level scheme for observing quantum beats. Excited states e_1 and e_2 are within the excitation bandwidth.

While time-resolved fluorescence spectroscopy involves an excitation polarization and a detection polarization, pump/probe spectroscopy can actually employ three different polarizations: the pump polarization, the probe polarization, and the detection polarization. Consider, for instance, an experiment in which the pump is polarized at 0° ; we will call this polarization \hat{x} and horizontal polarization \hat{y} . The probe pulse is polarized at 45° ($[\hat{x} + \hat{y}]/\sqrt{2}$), and the detection polarizer at -45° ($[\hat{x} - \hat{y}]/\sqrt{2}$). An isotropic medium will not affect the polarization of the probe pulse, and so in the absence of the pump pulse no light will pass through the detection (or “analyzer”) polarizer. Following the pump pulse, the \hat{x} component of the probe pulse will experience a different change in absorption than the \hat{y} component, so that the probe pulse will no longer be polarized at 45° after the sample and some of it can therefore pass through the analyzer polarizer. The signal detected in this manner is called dichroism. The dichroism signal decays as reorientation (or other effects) bring the absorption changes in the \hat{x} and \hat{y} directions towards equality. Thus, a dichroism experiment allows for the observation of orientational dynamics in a single decay, rather than having to combine decays mathematically to calculate the time-dependent anisotropy. In addition, because no light passes through the analyzer polarizer in the absence of a pump pulse, dichroism is a zero-background technique, which is to say that the signal of interest appears alone rather than as a small change in the intensity of the probe beam.

We now consider the effects of changes in refractive index induced by the pump beam. The most common technique used to study refractive index changes is optical Kerr effect (OKE) spectroscopy.[15-18] OKE spectroscopy is generally performed in a liquid that is transparent at the pump and probe wavelengths. The pump pulse induces a change in the refractive index that can have both an isotropic component (i.e., one that is independent of probe polarization) and an anisotropic component (i.e., a birefringence).

20. Techniques for Ultrafast Spectroscopy

This refractive index change occurs via a number of different mechanisms, as shown in the typical OKE data in Fig. 20.7. When the pump pulse is present, it distorts the electron clouds of the molecules, leading to what is known as the electronic response. The pump pulse also initiates coherent vibration in the sample, both in intramolecular and intermolecular modes. These vibrations in turn modulate the refractive index of the sample until they have dephased. Finally, the pump beam also induces torque on molecules with anisotropic polarizabilities, making them tend to realign so as to have the greatest possible projection of their most polarizable axis along the polarization vector of the pump beam. This small induced alignment leads to a bire-



fringence that then decays via orientational diffusion.

Fig. 20.7. OKE decay for neat chloroform at room temperature. The sharp feature at zero delay time is the electronic response. The fast decay over the first picosecond is due to the dephasing of intermolecular vibrations. The oscillations arise from Raman-active intramolecular vibrational modes. The exponential decay at long times is due to orientational diffusion.

There are many possible implementations of OKE spectroscopy, the most common of which is a polarization spectroscopy setup that is similar to the setup discussed above for measuring dichroism. The pump pulse is polarized at 0° and the probe at 45° . The probe passes through an analyzer polarizer set at -45° after the sample. Thus, unless the pump beam induces birefringence in the sample, no signal will be detected. This polarization spectroscopy setup therefore measures the anisotropic portion of the change in the refractive index.

Standard polarization spectroscopy measures the intensity of the signal, which is to say the magnitude squared of the signal electric field. Being able to measure the signal electric field directly can also be desirable at times. One method of doing so is known as optical heterodyne detection

20. Techniques for Ultrafast Spectroscopy

(OHD).[19, 20] In an OHD-OKE experiment, a quarter-wave plate is inserted into the probe path directly before the polarizer that is used to set the probe polarization (Fig. 20.8). The quarter-wave plate is adjusted so that its fast axis is along the direction of the polarization passed by the polarizer. The polarizer is then rotated by a small amount, generally on the order of 1° . As a result, some light passes through the analyzer polarizer. Since the analyzer polarizer is aligned with the slow axis of the quarter-wave plate, the light that gets through the analyzer is 90° out of phase with the light that does not get through it. The light that leaks through the analyzer polarizer is known as the local oscillator. Because the OKE signal arises from changes in index of refraction, it is also 90° out of phase with the probe beam, but it is in phase with the local oscillator (LO). Thus, the total electric-field intensity at the detector is given by

$$I = (E_{LO} + E_{sig})(E_{LO} + E_{sig})^* = I_{LO} + 2E_{LO}E_{sig} + I_{sig}, \quad (20.14)$$

where we have made use of the fact that E_{LO} and E_{sig} have the same phase. In general, $I_{LO} \gg 2E_{LO}E_{sig} \gg I_{sig}$, so the last of these terms can be ignored. Because I_{LO} does not oscillate at the frequency at which the pump beam is chopped, lock-in detection can be employed to isolate the $2E_{LO}E_{sig}$ term. It is therefore clear from the above inequality that the local oscillator effectively amplifies the electric field of interest and also linearizes it.

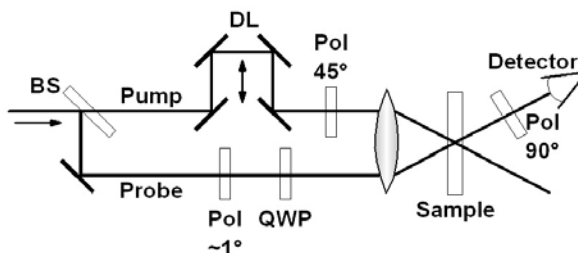


Fig. 20.8. Schematic setup for optical heterodyne detection in OKE spectroscopy. BS = beam splitter, DL = delay line, Pol = polarizer, QWP = quarter-wave plate.

The electronic response in OKE spectroscopy, which in effect tracks the shape of the laser pulses, is one example of what is often called a “coherence spike.” Coherence spikes occur in all nonlinear spectroscopies, and are a consequence of the additional processes that can occur when more than one laser pulse is present at the same time. Because of coherence spikes, great caution should be exercised in drawing any conclusions regarding dynamics that may occur on a time scale comparable to or faster than the duration of the laser pulses used for an experiment.

20. Techniques for Ultrafast Spectroscopy

There are many varieties of pump/probe spectroscopy beyond those covered here. Other transient effects can be probed, such as changes in reflectivity [21] or circular dichroism.[22] There are also other experimental arrangements that can be used for specific measurements. For instance, the setup for OKE spectroscopy described above only measures the anisotropic response, and a different setup is required to measure the isotropic response. While there is not space here to discuss the spectroscopies in the pump/probe family exhaustively, the discussion here should give the reader a good flavor for the basics of any of these techniques.

The Transient Grating

Another popular ultrafast spectroscopic technique is the transient grating (TG).[23, 24] TG spectroscopy is closely related to pump/probe spectroscopy, except that two pump pulses are employed instead of one. The two pump pulses come from the same laser. They cross at some angle θ and are time-coincident at the sample. Because the beams meet at an angle, they create interference fringes in the crossing volume. If the beams have wavevectors \mathbf{k}_1 and \mathbf{k}_2 , then the interference pattern will have a wavevector given by

$$\mathbf{k}_{grating} = \mathbf{k}_1 - \mathbf{k}_2 . \quad (20.15)$$

In other words, the two excitation pulses can be thought of as creating a grating with a fringe spacing d given by

$$d = \frac{\lambda}{2\sin(\theta/2)} . \quad (20.16)$$

This grating can be “written” within the sample in any of a number of ways, including changes in absorption or in refractive index.

Once the grating has been written in the sample, it can be probed by a third pulse that is delayed in time from the excitation pulses. The probe pulse can come from the same laser as the pump pulses or from a different laser. It must approach the grating at an angle that satisfies the Bragg condition, i.e.

$$\theta_{probe} = 2\sin^{-1}\left(\frac{\lambda_{probe}}{2d}\right) . \quad (20.17)$$

If this condition is met, then the probe beam can diffract off of the grating, creating a signal beam with a wavevector given by

$$\mathbf{k}_{signal} = \mathbf{k}_1 - \mathbf{k}_2 + \mathbf{k}_{probe} . \quad (20.18)$$

20. Techniques for Ultrafast Spectroscopy

Thus, one advantage of TG spectroscopy, as opposed to pump/probe spectroscopy, is that the signal travels in a unique direction rather than along with the probe beam.

A typical TG setup is shown in Fig. 20.9. The two excitation beams travel parallel to one another and are focused into the sample with a lens. The probe beam (if it is the same color as the excitation beams) travels either directly above or directly below one of the excitation beams, so that the beams define three corners of a rectangle. After the sample, the signal beam appears in the fourth corner of the rectangle.

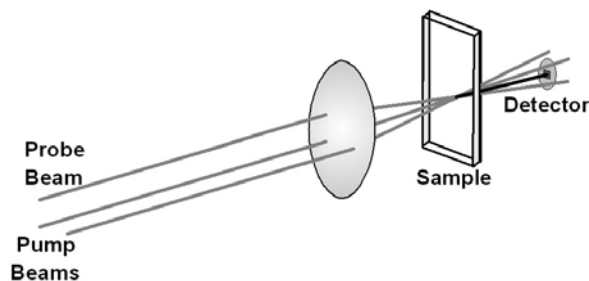


Fig. 20.9. Schematic setup for a TG experiment. The probe beam usually traverses a delay line, whereas the pump pulses remain fixed in time. The signal beam (black line) is diffracted in a unique direction for background-free detection.

Another approach to TG spectroscopy that is gaining popularity is to use diffractive optics to create and probe the TG (Fig. 20.10).[25, 26] In this scheme, a single excitation beam is incident on a transmission grating. The grating is imaged onto the sample, and all of the diffracted spots other than the first-order spots are blocked. The probe beam is created in the same manner, such that it automatically meets the Bragg condition for the TG. One of the first-order diffraction spots from the probe beam can be blocked so that there is only a single probe beam. Alternatively, the second first-order diffraction spot can be imaged on the sample as well and used as a local oscillator for the signal. The phase of this local oscillator relative to the signal can be adjusted by placing a glass flat in the beam path and controlling its orientation.

The diffractive-optic approach to TG spectroscopy has the disadvantage that it throws away light from unused diffraction orders. However, this problem can be minimized by using a high-quality transmission grating that has a sinusoidal variation in refractive index. Diffractive optics also make it more difficult to implement complete polarization control. However, the ease with which the setup can be aligned and with which heterodyne detection can be incorporated in a diffractive-optic setup are significant advantages. Furthermore, changing the fringe spacing is a simple matter of using a different grating on the same substrate, whereas the conventional approach

20. Techniques for Ultrafast Spectroscopy

requires significant realignment of optics every time the fringe spacing is changed.

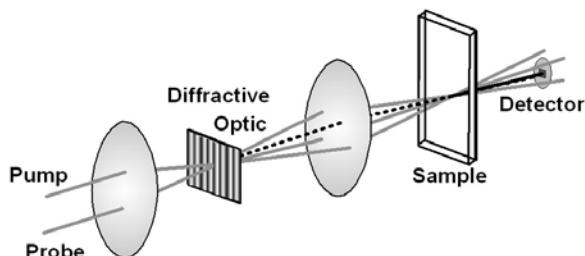


Fig. 20.10. Schematic setup for TG spectroscopy using a diffractive optic. One of the diffracted beams (dashed line) acts as a local oscillator for the signal beam (solid black line).

Because TG spectroscopy involves three laser beams and a signal beam, there are four polarizations involved, affording many opportunities for selectively enhancing or suppressing particular contributions to the signal.[27, 28] For instance, if both pump beams are polarized at 0° and the probe and signal are polarized at the magic angle, the effects of reorientation can be removed from the TG decay.

The configuration in which both excitation beams have the same polarization is often called an intensity grating.[29] As discussed above, this configuration leads to a sinusoidal modulation of the intensity along the grating wavevector. Another commonly-used configuration employs orthogonally-polarized excitation pulses. In this case it is not the intensity that is modulated along the grating wavevector, but rather the polarization. Across one period of the grating the polarization changes from right circular to linear at 45° to left circular to linear at -45° to right circular (Fig. 20.11).[29] As a result, this configuration is often called a polarization grating. If the probe polarization is vertical, then the signal generated from the polarization grating will be horizontal (and vice versa).



Fig. 20. 11. Variation of the polarization across one fringe of a polarization grating.

As an example of an application of a polarization grating, consider performing TG spectroscopy on a dye solution. If an intensity grating is created, then a spatially-modulated population of excited molecules will be created. The decay of this grating will occur through both reorientation and relaxation of the excited states. In analogy to what we have seen for

pump/probe spectroscopy, reorientation will lead to a partial decay of the signal. On the other hand, population relaxation will cause the grating to decay completely. By probing at the magic angle, the population decay time can be measured. Again in analogy to pump/probe spectroscopy, the reorientation time can then be determined by making two more intensity-grating measurements to determine the time-dependent anisotropy. If a polarization grating is created in the same medium, there will be no spatial modulation in the excited-state population. Instead, the spatial modulation will be in the initial orientation of excited molecules. As a result, both reorientation and population relaxation will cause the signal to decay completely, and so the relaxation rate will be the sum of the rates of both of these processes. Thus, if the population-relaxation time has been measured by probing an intensity grating at the magic angle, then the orientational relaxation time can be determined from a single polarization-grating measurement.

More complex polarization schemes can also be used for excitation and probing. For example, using one excitation beam polarized at 0° , one excitation beam polarized at 45° , and a probe beam polarized at 90° makes it possible to suppress different contributions to TG OKE signal simply by choosing the polarization that is detected.[28] Under these conditions, detecting the signal at -45° suppresses the electronic OKE response and detecting the signal at 56.3° suppresses the nuclear OKE signal. Different detection polarizations are useful for suppressing other contributions to the TG signal.

Essentially any measurement that can be made using pump/probe spectroscopy can also be made with TG spectroscopy, thereby gaining all of the advantages of TG spectroscopy discussed above. However, the greatest advantage of TG spectroscopy is that it allows for additional types of phenomena to be probed based upon the spatial scale imposed by the grating wavevector.

One example of a phenomenon that can be monitored with TG spectroscopy is diffusion.[30] An intensity grating gets washed out as excited molecules move from bright regions of the grating to dark regions, and as unexcited molecules do the opposite. If this motion occurs diffusively, then its contribution to the grating decay is proportional to $\exp(-2t\Delta^2D)$, where $\Delta = 2\pi/d$ and D is the diffusion constant. Thus, a plot of the grating decay rate as a function of $1/d^2$ can be used to determine the diffusion constant of a species. Of course, this measurement is limited by the lifetime of the excited species, but this problem can be circumvented by, for instance, using the excitation pulses for permanent photobleaching of the species for which the diffusion constant is to be determined.

Another example of an effect that takes advantage of the spatial dependence of the TG excitation process is acoustic spectroscopy.[31, 32] At the bright regions in an intensity grating, processes such as heating and electrostriction can lead to transient density changes. Because these density changes vary sinusoidally in space, they are equivalent to an acoustic stand-

20. Techniques for Ultrafast Spectroscopy

ing wave. As a result, the TG excitation step can launch counterpropagating acoustic waves along the grating wavevector. The acoustic waves in turn modulate the index of refraction of the grating in a time-dependent manner, creating oscillations in the TG decay (Fig. 20.12).[33, 34] The frequency of these oscillations is determined by the grating fringe spacing and the sound velocity of the medium. Being able to measure the acoustic dispersion of a medium can be of great use in determining its mechanical properties.

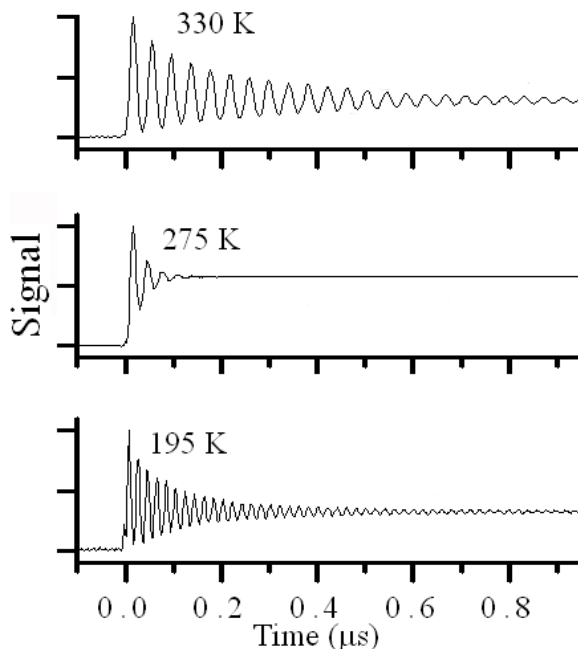


Fig. 20.12. TG data for glycerol at a set fringe spacing but different temperatures. In the upper panel the acoustic oscillations show liquid-like behavior. In the center panel the liquid is supercooled. In this case the acoustic period is comparable to the characteristic decay time of the liquid, and so the oscillations are highly damped. In the lower panel the glycerol is a glass, and the acoustic data are characteristic of a solid. Data courtesy of Keith A. Nelson.

Coherent Anti-Stokes Raman Spectroscopy

Coherent Anti-Stokes Raman Spectroscopy (CARS) is another ultrafast spectroscopic technique that is related to pump/probe spectroscopy.[17, 35, 36] As in the case of TG spectroscopy, CARS involves two time-coincident pump pulses. However, in CARS the pulses are of two different colors, ω_1 and ω_2 , and the energy difference $\omega_1 - \omega_2$ matches a Raman

20. Techniques for Ultrafast Spectroscopy

transition frequency in the sample of interest (Fig. 20.13a). Thus, the excitation step creates a coherence between two vibrational states of the molecule. The probe pulse arrives at the sample after a delay time τ . The probe pulse generally is of frequency ω_1 , in which case a signal is generated at new frequency $\omega_{sig} = 2\omega_1 - \omega_2$. The intensity of this signal is a measure of the degree of vibrational coherence remaining after delay time τ , and so CARS is a useful means of studying vibrational dynamics.

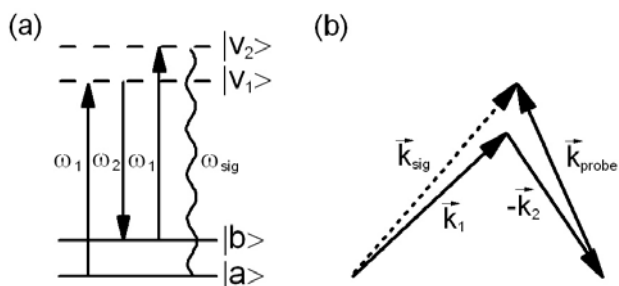


Fig. 20.13. (a) Energy-level scheme for CARS. $|a\rangle$ and $|b\rangle$ are the ground vibrational state and an excited vibrational state, respectively, and $|v_1\rangle$ and $|v_2\rangle$ are virtual electronic states. (b) Phase-matching diagram for CARS.

Because CARS involves two excitation colors, phase matching is a more challenging problem than for the spectroscopies that we have discussed so far. The phase-matching condition (Fig. 20.13b) is that

$$\mathbf{k}_{signal} = \mathbf{k}_1 - \mathbf{k}_2 + \mathbf{k}_{probe} . \quad (20.19)$$

The problem of meeting this condition is compounded when the vibration being studied is of high frequency, as dispersion in the sample may need to be taken into account as well in choosing the experimental geometry.

Because the bandwidths of Raman transitions are generally on the order of 10 cm^{-1} or less, it is desirable to use laser pulses with durations in the range of a few picoseconds for CARS. If shorter pulses are employed, much of the laser bandwidth does not go into generating signal, and so the efficiency of the CARS process is reduced.

As is the case with all of the other coherent spectroscopies that we have discussed, there can be a coherence spike in CARS. In this spectroscopy, the coherence spike arises from having two consecutive upward transitions followed by a downward transition (Fig. 20.14). Note that this process does not depend upon any vibrational resonance, and so it can happen in any molecule. However, since it has no resonant step, the coherence spike is also 90° out of phase with the desired CARS signal. In applications of CARS in

which all of the pulses arrive at once, such as many implementations of CARS microscopy, this effect is also called the “nonresonant background.”

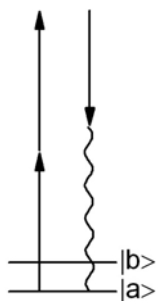


Fig. 20.14. Energy-level diagram for the nonresonant background signal in CARS.

Since CARS generally involves three laser pulses and a signal, up to four different polarizations can be employed. As with the other spectroscopies discussed above, the CARS signal is affected by reorientation. Polarizing both excitation pulses at 0° and detecting and probing at the magic angle removes the effects of reorientation from the CARS decay. As was the case in OKE spectroscopy, this configuration probes only the isotropic portion of the signal. Similarly, having excitation beams polarized at 0° and 90° , a probe beam polarized at 0° , and detecting at 90° polarization measures only the anisotropic portion of the CARS response. Which of these responses dominates is highly dependent on the geometry of the vibrational mode being studied. Other polarization conditions can be employed to suppress the nonresonant background, if desired.[37]

Photon Echo Spectroscopy

The mechanisms for broadening of linear spectra can be divided, more or less, into two categories: homogeneous and inhomogeneous. Homogeneous broadening mechanisms can be defined roughly as those processes that contribute to the width of the spectrum of a single molecule, such as population relaxation and dephasing. Inhomogeneous broadening arises when different molecules in an ensemble have different transition frequencies, as can happen via Doppler broadening or from the distribution of different environments in a solution. Of course, the transition frequency of a molecule can also change over time, and so the dividing line between homogeneous and inhomogeneous processes also depends on the time scale in question.

20. Techniques for Ultrafast Spectroscopy

Linear spectroscopy cannot discriminate between inhomogeneous and homogeneous broadening. However, this distinction can be made using photon echo (PE) spectroscopy,[38, 39] an optical analog of spin echo spectroscopy in nuclear magnetic resonance. In PE spectroscopy, a laser pulse creates a coherence between the ground and excited states of the molecules in a system. This coherence evolves at frequency $\omega_{eg} = (E_e - E_g)/\hbar$, where e and g signify the excited and ground states, respectively. In the presence of inhomogeneous broadening, the system will have some distribution of transition frequencies ω_{eg} .

After the first pulse, the system is allowed to evolve for a delay time τ , such that in the absence of homogeneous broadening each molecule accumulates a phase $\omega_{eg}\tau$ according to its transition frequency. A second laser pulse then switches the coherence to evolve at frequency $\omega_{ge} = -\omega_{eg}$. After a second delay period of τ , each molecule has accumulated a total phase of $\omega_{eg}\tau - \omega_{eg}\tau = 0$. Thus, at time 2τ coherence has been restored (barring any dephasing that has occurred via homogeneous mechanisms) and the system can radiate a coherent signal. The signal is collected as a function of the delay time τ , and the resultant decay gives a picture of the homogeneous relaxation dynamics.

In a PE experiment, the phase-matching condition is

$$\mathbf{k}_{signal} = \mathbf{k}_1 - 2\mathbf{k}_2, \quad (20.20)$$

where 1 and 2 refer to the first and second pulses, respectively. Thus, if the two beams cross at a small angle θ , then signal beams will be found approximately angle θ over from each of the excitation beams. At room temperature in condensed phases, homogeneous relaxation often occurs on a time scale of tens of femtoseconds. In such cases it is useful to collect both echo signals so that zero delay time can be determined accurately.

A more sophisticated version of this experiment is the three-pulse or stimulated photon echo. In the three-pulse echo, the first pulse creates a coherence at frequency ω_{eg} . The second pulse, which comes at delay time τ , converts this coherence into a population. After waiting time T , a third pulse converts the population into a coherence at frequency ω_{ge} , after which an echo is emitted. The stimulated echo makes it possible to monitor frequency variations (also known as “spectral diffusion”) on time scales longer than the dephasing time of coherences.

The phase matching condition for the stimulated echo is

$$\mathbf{k}_{signal} = \mathbf{k}_1 - \mathbf{k}_2 - \mathbf{k}_3. \quad (20.21)$$

In the most common configuration for this experiment, the first two beams are separated by a small angle θ in the same horizontal plane, and the third beam is between them but displaced vertically (Fig. 20.15). Two signal beams are again generated. Often both of these beams are monitored. Generally the population time T is fixed and the coherence time τ is scanned. The spacing between the peaks of the two signals in the scans of τ is then determined as a function of T in a so-called three-pulse echo peak shift (3PEPS) experiment.[40]

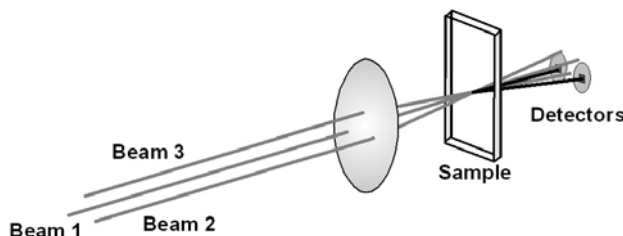


Fig. 20.15. Schematic experimental layout for 3PEPS.

Surface-Selective Spectroscopies

The nonlinear optical spectroscopies that we have discussed so far are all four-wave-mixing techniques, which is to say that they depend upon the third-order optical response function, $R^{(3)}$ (which is related to the third-order optical susceptibility $\chi^{(3)}$).[41] Why is it that we have discussed linear techniques and third-order techniques but not second-order techniques? Within the electric dipole approximation, an optical signal can only be produced in isotropic media that have inversion symmetry (such as bulk liquids) if each polarization index (x , y or z) in the response function appears an even number of times. For instance, linear spectroscopy depends upon the first-order optical response $R^{(1)}$, which has two polarization indices (one for the incoming light and one for the signal). Similarly, third-order techniques have four polarization indices, and so elements of the third-order response tensor in which each spatial index appears an even number of times can be observed in isotropic media. The second-order optical response function has three polarization indices, and so it is impossible for at least one of the spatial indices to appear an even number of times. As a result, second-order techniques do not produce signals in centrosymmetric media.[41]

The fact that nonlinear-optical techniques that depend on even-order response functions are not allowed in isotropic media is tremendously useful. Because inversion symmetry is necessarily broken at the boundary between two media, it is possible to probe interfaces selectively with such spectroscopies.[42-47] Such experiments generally employ ultrafast lasers, which

have high enough intensities that appreciable signals can be generated despite the relatively small number of molecules at an interface.

If the media on both sides of an interface are isotropic, then inversion symmetry is broken only along the normal to the interface. This direction is generally denoted z . It is the z polarization index that is allowed to appear an odd number of times in an even-order response function or susceptibility. For instance, the elements of $\chi^{(2)}$ that are non-zero at such an interface are $\chi^{(2)}_{xxz} = \chi^{(2)}_{yyz}$, $\chi^{(2)}_{xzx} = \chi^{(2)}_{yzy}$, $\chi^{(2)}_{zxx} = \chi^{(2)}_{zyy}$, and $\chi^{(2)}_{zzz}$. Since each of these tensor elements contains at least one factor of z , at least one input beam or signal beam must have a projection of its polarization along the z axis. This requirement means that the beams in second-order spectroscopies generally are not normal to the interface. The input beams and signal generally lie in a single plane that is perpendicular to the plane of the interface. Light that is polarized within the plane defined by the beams (this polarization is denoted P) has a z component, whereas light that is polarized perpendicularly to this plane (this polarization is denoted S) has no z component. The allowed polarization combinations are thus SSP , SPS , PSS and PPP , where the list of polarizations, by convention, begins with that of the signal.[48]

What does it mean for inversion symmetry to be broken at an interface? In the simplest sense, inversion symmetry is broken because there are different media on each side of the interface. However, we should really think about the symmetry problem in terms of the species that generate the signal, which are generally either molecules (as in a liquid) or specific chemical groups (such as those that may decorate the surface of a solid substrate). To a first approximation, if as many molecules (or chemical groups) point along z as point along $-z$, then we would not expect a signal to be generated. Thus, for instance, a liquid composed of centrosymmetric molecules might not be expected to generate a $\chi^{(2)}$ signal at an interface. Of course, the presence of the interface may in itself break the symmetry of the molecule, insofar as each side of the molecule is in a different chemical environment. Nevertheless, even under such circumstances the $\chi^{(2)}$ signal would be expected to be weak. Thus, $\chi^{(2)}$ spectroscopies are powerful tools for studying orientations of molecules at interfaces.

The simplest $\chi^{(2)}$ spectroscopy is surface second-harmonic generation (SHG).[42, 47, 49] Generally in this technique, a single ultrafast laser beam is employed. The sample under study is usually completely transparent at the laser wavelength. The laser beam approaches the interface at an angle to the normal (Fig. 20.16), and the SHG signal is collected either in transmission or reflection. The strength of the SHG signal is dependent on the degree of ordering of molecules at the interface. By varying the laser and detection polarizations it is possible to gain significant insight into this molecular ordering. SHG can also have some degree of molecular specificity if there is a species that has an electronic absorption that is near to resonance with two photons of the excitation source, a condition that greatly increases the signal strength.

20. Techniques for Ultrafast Spectroscopy

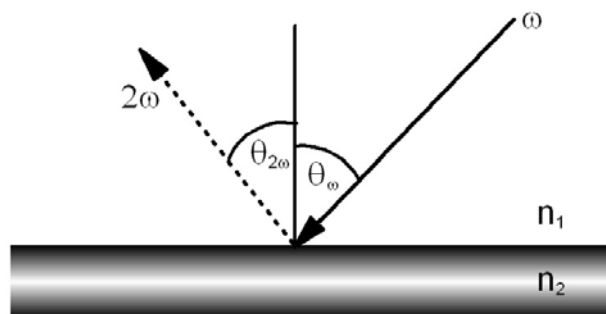


Fig. 20.16. Schematic experimental geometry for surface SHG spectroscopy in reflection mode. The input beam at frequency ω makes angle θ_ω with the surface normal, and the signal beam of frequency 2ω makes angle $\theta_{2\omega}$ with the surface normal. The refractive indices of the two media at the interface are n_1 and n_2 .

While for many years the majority of surface-selective $\chi^{(2)}$ experiments involved SHG, the increased availability of high-quality, ultrafast, infrared laser sources over the past decade has facilitated the development of surface-selective, $\chi^{(2)}$ vibrational spectroscopies.[42, 45, 48] While it is possible to perform either sum-frequency or difference-frequency generation at interfaces, for practical reasons it is the former technique that is almost universally employed. Vibrational sum-frequency spectroscopy (VSFS) employs an ultrafast infrared laser as well as a visible ultrafast laser tuned to a wavelength at which the sample is transparent. The two laser beams cross at a point on the interface of interest (Fig. 20.17) at angles to the surface normal that allow for good phase matching of the signal. The signal at frequency $\omega_{signal} = \omega_{IR} + \omega_{visible}$ is usually collected in reflection. When the infrared laser frequency is resonant with a vibrational mode at the interface, there is a strong enhancement of the VSFS signal, allowing for the collection of vibrational spectra of those molecules at the interface of interest. As was the case for surface SHG spectroscopy, the strength of the signal depends intimately on the details of the molecular organization at the interface. Because it is a vibrational spectroscopy, VSFS offers considerably more molecular selectivity than does surface SHG spectroscopy. In addition, VSFS can be used to probe multiple vibrational modes in a single species, allowing for the development of a much more detailed picture of the surface molecular organization.

20. Techniques for Ultrafast Spectroscopy

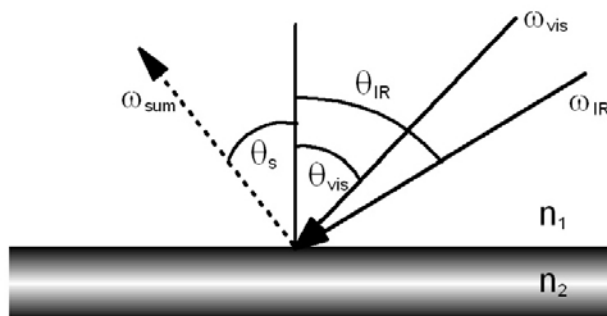


Fig. 20.17. Schematic experimental geometry for vibrational sum-frequency generation in reflection mode.

By convention, the polarizations for VSFS experiments are listed in the order signal, visible, infrared. The *SSP* polarization combination is the one that is used most commonly. This combination generally yields the strongest (and most readily interpretable) VSFS signal, as it relies upon the mode of interest having a projection of its IR transition moment along the *z* axis. However, obtaining VSFS data using additional polarization combinations can also be useful for the more accurate determination of molecular orientation.

VSFS experiments are generally performed with the visible and IR pulses overlapped in time. Under these conditions, non-resonant background signal is also created, as was the case in CARS spectroscopy. The processes that lead to the non-resonant background are shown in Fig. 20.18. These processes are weak due to their lack of vibrational resonance, but by the same token they can occur for any and every molecule at an interface.

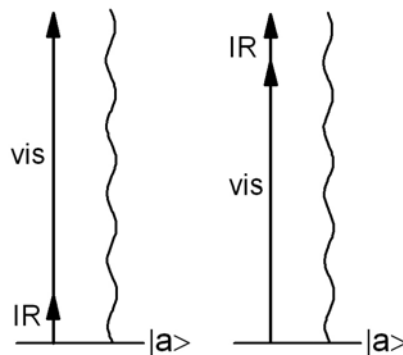


Fig. 20.18. Energy-level diagrams of the pathways contributing to the nonresonant background in vibrational sum-frequency generation spectroscopy.

References

1. Valeur, B., *Molecular Fluorescence: Principles and Applications*. 2001, Weinheim: Wiley-VCH.
2. Lakowicz, J.R., *Principles of Fluorescence Spectroscopy*. 2 ed. 1999, Berlin: Springer.
3. O'Connor, D.V. and D. Phillips, *Time-Correlated Single Photon Counting*. 1984, New York: Academic Press.
4. Becker, W., *Advanced Time-Correlated Single Photon Counting Techniques*. Springer Series in Chemical Physics. 2005, Berlin: Springer.
5. Tomov, I.V., R. Fedosejevs, and A.A. Offenberger, *Upconversion of Subpicosecond Light-Pulses*. Ieee Journal of Quantum Electronics, 1982. **18**(12): p. 2048-2056.
6. Kahlow, M.A., et al., *Ultrafast Emission-Spectroscopy in the Ultraviolet by Time-Gated Upconversion*. Review of Scientific Instruments, 1988. **59**(7): p. 1098-1109.
7. Tao, T., *Time-Dependent Fluorescence Depolarization and Brownian Rotational Diffusion Coefficients of Macromolecules*. Biopolymers, 1969. **8**: p. 609-632.
8. Glasbeek, M. and H. Zhang, *Femtosecond Studies of Solvation and Intramolecular Configurational Dynamics of Fluorophores in Liquid Solution*. Chemical Reviews, 2004. **104**(4): p. 1929-1954.
9. Barbara, P.F. and W. Jarzeba, *Ultrafast Photochemical Intramolecular Charge and Excited State Solvation*. Advances in Photochemistry, 1990. **15**: p. 1-68.
10. Barbara, P.F., et al., *Solvation Dynamics and Ultrafast Electron Transfer*, in *Perspectives in Photosynthesis*, J. Jortner and B. Pullman, Editors. 1990, Kluwer: Deventer. p. 273-292.
11. Castner, E.W., Jr., et al., *The Dynamics of Polar Solvation*. Ber. Bunsen-Ges. Phys. Chem., 1988. **92**(3): p. 363-72.
12. Mukamel, S., *Principles of Nonlinear Optical Spectroscopy*. 1995, New York: Oxford University Press. 543.
13. Vanamerongen, H. and R. Vangrondelle, *Transient Absorption-Spectroscopy in Study of Processes and Dynamics in Biology*, in *Biochemical Spectroscopy*. 1995. p. 201-226.
14. Henriksen, N.E. and V. Engel, *Femtosecond Pump-Probe Spectroscopy: A Theoretical Analysis of Transient Signals and Their Relation to Nuclear Wave-Packet Motion*. International Reviews in Physical Chemistry, 2001. **20**(2): p. 93-126.
15. Righini, R., *Ultrafast Optical Kerr Effect in Liquids and Solids*. Science, 1993. **262**: p. 1386-1390.

20. *Techniques for Ultrafast Spectroscopy*

16. Kinoshita, S., et al., *Low Frequency Modes Probed by Time-Domain Optical Kerr Effect Spectroscopy*. International Journal of Modern Physics B, 1996. **10**(11): p. 1229-1272.
17. Fourkas, J.T., *Nonresonant Intermolecular Spectroscopy of Liquids*, in *Ultrafast Infrared and Raman Spectroscopy*, M.D. Fayer, Editor. 2001, Marcel Dekker: New York. p. 473-512.
18. Smith, N.A. and S.R. Meech, *Optically-Heterodyne-Detected Optical Kerr Effect (OHD-OKE): Applications in Condensed Phase Dynamics*. International Reviews in Physical Chemistry, 2002. **21**(1): p. 75-100.
19. McMorro, D., *Separation of Nuclear and Electronic Contributions to Femtosecond Four-Wave Mixing Data*. Optics Communications, 1991. **86**: p. 236-244.
20. McMorro, D. and W.T. Lotshaw, *Intermolecular Dynamics in Acetonitrile Probed with Femtosecond Fourier Transform Raman Spectroscopy*. Journal of Physical Chemistry, 1991. **95**: p. 10395-10406.
21. Harata, A., Q. Shen, and T. Sawada, *Photothermal Applications of Lasers: Study of Fast and Ultrafast Photothermal Phenomena at Metal-Liquid Interfaces*. Annual Review of Physical Chemistry, 1999. **50**: p. 193-219.
22. Fischer, P. and F. Hache, *Nonlinear Optical Spectroscopy of Chiral Molecules*. Chirality, 2005. **17**(8): p. 421-437.
23. Eichler, H.J., P. Günter, and D.W. Pohl, *Laser-Induced Dynamic Gratings*. 1986, New York: Springer-Verlag.
24. Fourkas, J.T. and M.D. Fayer, *The Transient Grating: A Holographic Window to Dynamic Processes*. Accounts of Chemical Research, 1992. **25**: p. 227-233.
25. Goodno, G.D., G. Dadusc, and R.J.D. Miller, *Ultrafast Heterodyne-Detected Transient-Grating Spectroscopy Using Diffractive Optics*. Journal of the Optical Society of America B, 1998. **15**(6): p. 1791-1794.
26. Maznev, A.A., K.A. Nelson, and J.A. Rogers, *Optical Heterodyne Detection of Laser-Induced Gratings*. Optics Letters, 1998. **23**(16): p. 1319-1321.
27. Etchepare, J., et al., *Polarization Selectivity in Time-Resolved Transient Phase Grating*. Optics Communications, 1987. **63**(5): p. 329-334.
28. Deeg, F.W. and M.D. Fayer, *Analysis of Complex Molecular Dynamics in an Organic Liquid by Polarization Selective Subpicosecond Transient Grating Experiments*. Journal of Chemical Physics, 1989. **91**(4): p. 2269-2279.
29. Fourkas, J.T., R. Trebino, and M.D. Fayer, *The Grating Decomposition Method: A New Approach for Understanding Polarization-Selective Transient Grating Experiments. I. Theory*. Journal of Chemical Physics, 1992. **97**(1): p. 69-77.

20. Techniques for Ultrafast Spectroscopy

30. Rose, T.S., et al., *Gas Phase Dynamics and Spectroscopy Probed with Picosecond Transient Grating Experiments*. Journal of Chemical Physics, 1987. **86**(10): p. 5370-5391.
31. Miller, R.J.D., et al., *Laser-Induced Ultrasonics: A Dynamic Holographic Approach to the Measurement of Weak Absorptions, Photoelastic Constants, and Acoustic Attenuation*. Chemical Physics, 1982. **72**: p. 371-379.
32. Nelson, K.A., et al., *Optical Generation of Tunable Ultrasonic Waves*. Journal of Applied Physics, 1982. **53**(2): p. 1144-1149.
33. Yan, Y.-X., L.-T. Cheng, and K.A. Nelson, *The Temperature-Dependent Distribution of Relaxation Times in Glycerol: Time-Domain Light Scattering Study of Acoustic and Mountain-Mode Behavior in the 20 MHz-3 GHz Frequency Range*. Journal of Chemical Physics, 1988. **88**(10): p. 6477-6486.
34. Paolucci, D.M. and K.A. Nelson, *Impulsive Stimulated Thermal Scattering Study of Structural Relaxation in Supercooled Glycerol*. Journal of Chemical Physics, 2000. **112**(15): p. 6725-6732.
35. Tolles, W.M., et al., *Review of Theory and Application of Coherent Anti-Stokes Raman-Spectroscopy (CARS)*. Applied Spectroscopy, 1977. **31**(4): p. 253-271.
36. Schmidt, S.C. and D.S. Moore, *Vibrational Spectroscopy of High-Temperature, Dense Molecular Fluids by Coherent Anti-Stokes-Raman Scattering*. Accounts of Chemical Research, 1992. **25**(9): p. 427-432.
37. Cheng, J.X., L.D. Book, and X.S. Xie, *Polarization Coherent Anti-Stokes Raman Scattering Microscopy*. Optics Letters, 2001. **26**(17): p. 1341-1343.
38. Kurnit, N.A., I.D. Abella, and S.R. Hartmann, *Observation of a Photon Echo*. Physical Review Letters, 1964. **13**(19): p. 567-568.
39. de Boeij, W.P., M.S. Pshenichnikov, and D.A. Wiersma, *Ultrafast Solvation Dynamics Explored by Femtosecond Photon Echo Spectroscopies*. Annual Reviews of Physical Chemistry, 1998. **49**: p. 99-123.
40. Nagasawa, Y., et al., *Temperature Dependence of Optical Dephasing in an Organic Polymer Glass (PMMA) from 300 K to 30 K*. Journal of Chemical Physics, 1997. **106**(12): p. 4840-4852.
41. Butcher, P.N. and D. Cotter, *The Elements of Nonlinear Optics*. Cambridge Studies in Modern Optics, ed. P.L. Knight and W.J. Firth. 1990, Cambridge: Cambridge University Press. 344.
42. Shen, Y.R., *Surface Properties Probed by Second-Harmonic and Sum-Frequency Generation*. Nature, 1989. **337**: p. 519-525.
43. Eienthal, K.B., *Liquid Interfaces*. Accounts of Chemical Research, 1993. **26**(12): p. 636-643.

20. Techniques for Ultrafast Spectroscopy

44. Raschke, M.B. and Y.R. Shen, *Nonlinear Optical Spectroscopy of Solid Interfaces*. Current Opinion In Solid State & Materials Science, 2004. **8**(5): p. 343-352.
45. Eienthal, K.B., *Liquid Interfaces Probed by Second-Harmonic and Sum-Frequency Spectroscopy*. Chemical Reviews, 1996. **96**(4): p. 1343-1360.
46. Richmond, G.L., *Molecular Bonding and Interactions at Aqueous Surfaces as Probed by Vibrational Sum Frequency Spectroscopy*. Chemical Reviews, 2002. **102**(8): p. 2693-2724.
47. Corn, R.M. and D.A. Higgins, *Optical 2nd-Harmonic Generation As a Probe of Surface-Chemistry*. Chemical Reviews, 1994. **94**(1): p. 107-125.
48. Zhuang, X., et al., *Mapping Molecular Orientation and Conformation at Interfaces by Surface Nonlinear Optics*. Physical Review B, 1999. **59**(19): p. 12632-12640.
49. Hicks, J.M., et al., *Studies of Liquid Surfaces by Second Harmonic Generation*. Journal of Physical Chemistry, 1986. **90**(4): p. 560-562.